Tethys, 5, 37–46, 2008
Journal of Weather & Climate of the Western Mediterranean
www.tethys.cat
ISSN-1697-1523
eISSN-1139-3394
DOI:10.3369/tethys.2008.5.04

Journal edited by **ACAM**
(Associació Catalana de Meteorologia)

# Merging micro-meteorology and Landsat imagery to monitor daily evapotranspiration at a regional scale

**J. M. Sánchez**[1], **V. Caselles**[1] **and G. Scavone**[2]

[1]Earth Physics and Thermodynamics Department, Universitat de València, C/ Dr. Moliner, 50, 46100 Burjassot, València
[2]Department of Engineering and Environmental Physics, University of Basilicata, Via N. Sauro 85, 85100 Potenza, Italy

Received: 9-I-2008 – Accepted: 15-IX-2008 – **Original version**

*Correspondence to:* Juan.M.Sanchez@uv.es

**Abstract**

*The objective of this work is to show the operational applicability of a recently proposed model (Sánchez et al., 2008) together with satellite images to monitor surface energy fluxes at a regional scale. In particular, we will focus on the retrieval of daily evapotranspiration because of the particular significance of this flux in the generation of precipitation or in agricultural water resource management. A detailed methodology to apply the Simplified Two- Source Energy Balance method to Landsat imagery is presented. The different surface cropland features are characterized from the CORINE Land Cover maps, and the required meteorological variables are obtained by interpolating the data of a network of agro-meteorological stations distributed within the region of interest. Finally, we show the application of the methodology to three different Landsat images covering the whole Basilicata region (Southern Italy). Maps of the different fluxes including the daily evapotranspiration are performed. Results are compared with some ground measurements, and an analysis is made taking the land use classification as a basis. An accuracy close to 30 W $m^{-2}$ is obtained.*

**Key words:** evapotranspiration, Landsat, Basilicata

## 1 Introduction

Evapotranspiration, $LE$, can be obtained on a local scale with an accuracy higher than 20% by well-known approaches such as the Penman-Monteith (PM) equation or the Priestley-Taylor (PT) method (Allen et al., 1998). Accurate measurements of air temperature and vapor pressure are required as inputs in the Penman-Monteith equation, and appropriate values of the Priestley-Taylor constant must be determined when applying this method to each particular area. Thus, these models cannot be applied on a regional scale unless we have a dense network of ground measurement stations. Moreover, most of them are models with a difficult application since they need too many measurements or parameter estimations. An attractive way to solve this problem is using remote sensing surface measurements. Remote sensing allows us to have information on many surface variables with a global coverage, after appropriate treatment and interpretation of the data registered by an instrument on board a satellite. Extension covered by a remote sensing image, and its spatial and temporal resolutions, depend on the sensor considered. There are sensors with a high spatial resolution but a low temporal one such as Landsat (spatial resolution of 30 m in the visible and 60 - 120 in the thermal infrared, and temporal resolution of 16 days) or ASTER (spatial resolution of 15 m in the visible and 90 m in the thermal bands and around 8 days frequency) and others with a higher overpass frequency but a lower spatial resolution such as MODIS (spatial resolution of 250 - 500 m in the visible and 1 km in the thermal bands and daily frequency), AVHRR (spatial resolution of 1.1 km and daily frequency), or AATSR (spatial resolution of 1 km and 2 - 6 days frequency). One of the goals of remote sensing is to provide us with data on barely accessible areas. This includes some regions such as, for example, forest areas where evapotranspiration retrieval is more difficult due to evident limitations on experiments.

The use of remote sensing techniques supplies the frequent lack of ground-measured variables and parameters re-

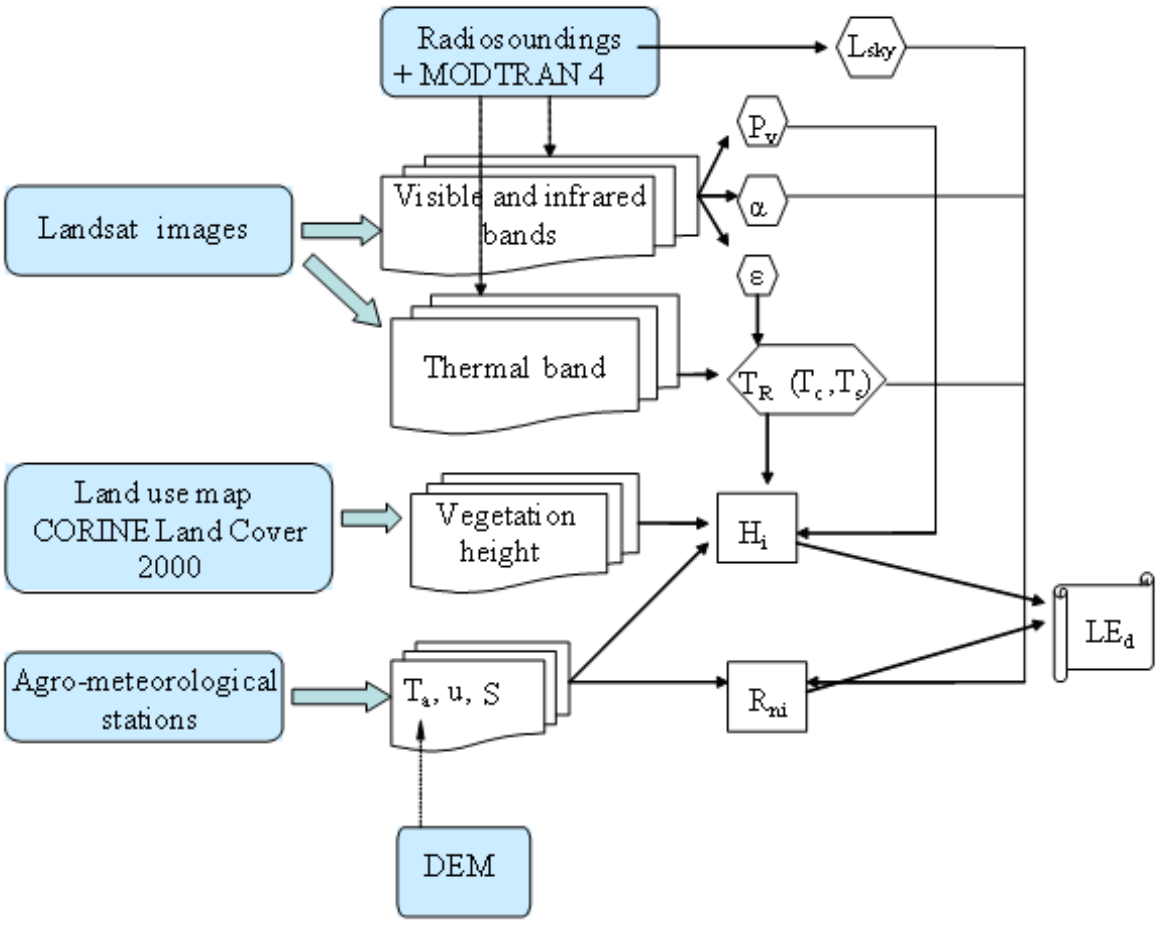


**Figure 1.** Scheme of the methodology proposed to retrieve actual daily evapotranspiration at a regional scale.

quired to apply the micro-meteorological models at a regional scale. Modelling evapotranspiration is very sensitive to the surface features and conditions. For this reason, a regional model must account for the surface variability. In this context, satellite remote sensing has become a basic tool since, as mentioned before, it allows us the regular monitoring of extensive areas. Different surface variables and parameters can be extracted from the combination of the multispectral information contained in a satellite image, and with a detail depending on the spatial resolution of the sensor used.

In this work, we show the application of the proposed Simplified Two-Source Energy Balance (STSEB) model (Sánchez et al., 2008) to the Basilicata region, in the south of Italy. This is a challenging region since it covers an extensive area with a large variety of land uses. The different surface features were characterized from the CORINE Land Cover land use maps (Büttner et al., 2002), and the required meteorological variables were obtained by interpolating the data of about forty agro-meteorological stations distributed within the region. Besides, atmospheric profiles from radiosoundings were used in the radiative transfer model MODTRAN 4.0 to correct the satellite data. Three satellite images were selected for this work, two from the Landsat 7-Enhanced Thematic Mapper (ETM+) (September 26th 1999 and June 14th 2002), and one from the Landsat 5-Thematic Mapper (TM) (May 26th 2004).

The main goal of this study is the union of a micrometeorological model and remote sensing techniques. The result of this combination is an operational methodology to retrieve daily evapotranspiration at a regional scale from remote sensing and local meteorological data. In this work we focus on the application of this methodology to Landsat imagery and a particular Italian region, but it could be extended to other high-resolution sensors, and what it is even more interesting, to any other regions in the world.

## 2 Methodology for estimating daily evapotranspiration using satellite remote sensing

Information of evapotranspiration at a daily scale is usually more interesting and useful than the instantaneous value at a particular time of day. However, when using high spatial

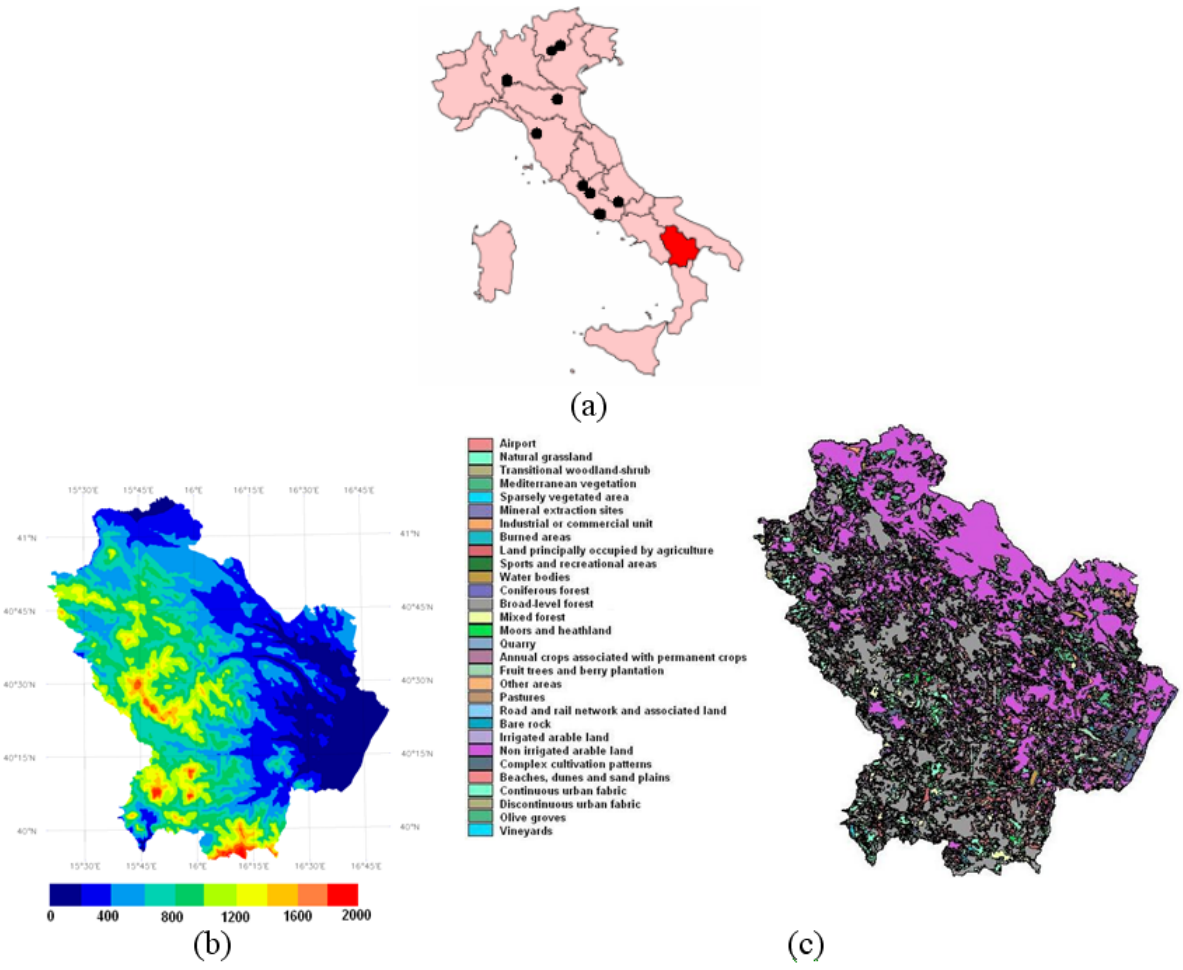


**Figure 2.** (a) Location of the Basilicata region. Black dots indicate the exact location of the different CarboEurope Italian sites. (b) Digital elevation model (m) of the Basilicata region. (c) Land use map of the Basilicata region (CORINE Land Cover 2000 project).

resolution satellites, only one image per day or less is acquired. Itier and Riou (1982) developed a simple procedure to calculate daily values of evapotranspiration from instantaneous flux values at a particular time of day. According to Itier and Riou (1982):

$$\frac{H_d}{R_{nd}} = \frac{H_i}{R_{ni}} \tag{1}$$

where $H$ is the sensible heat flux, $R_n$ is the net radiation flux, and the subscripts $i$ and $d$ refer to instantaneous and daily fluxes, respectively. Equation 1 implies that the Bowen ratio $\beta = H/LE$ is more or less constant throughout the day. This is not strictly true because $\beta$ is known to vary, especially at night. However, around midday the resulting errors are minor and most of satellite overpasses occur at this time. Sánchez et al. (2007) tested Equation 1 and observed good agreement in a range of 7 hours around midday.

At a daily scale the soil heat flux, $G$, can be neglected in the energy balance equation ($R_n = H + LE + G$), and $LE$ can be obtained from Equation 1 and the energy balance equation as:

$$LE_D = \frac{R_{nd}}{R_{ni}}(R_{ni} - H_i) \tag{2}$$

Using Equation 2, $LE_d$ can be obtained from the instantaneous values of $R_n$ and $H$ at a particular time of day, and the relative net radiation contribution at that time when global radiative exchange is integrated, $R_{nd}/R_{ni}$.

The sensible heat flux is obtained using the STSEB model described in Sánchez et al. (2008). In this paper, the method to estimate the net radiation can be simplified when the soil and canopy components are not required since it can be obtained using directly the effective values of surface temperature, $T_R$, albedo, $\alpha$, and emissivity, $\varepsilon$:

$$R_n = (1 - \alpha)S + \varepsilon L_{sky} - \varepsilon\sigma T_R^4 \tag{3}$$

where $S$ is the solar global radiation, and $\sigma$ is the Stefan-Boltzmann constant.

A scheme of the methodology proposed in this work is shown in Figure 1.

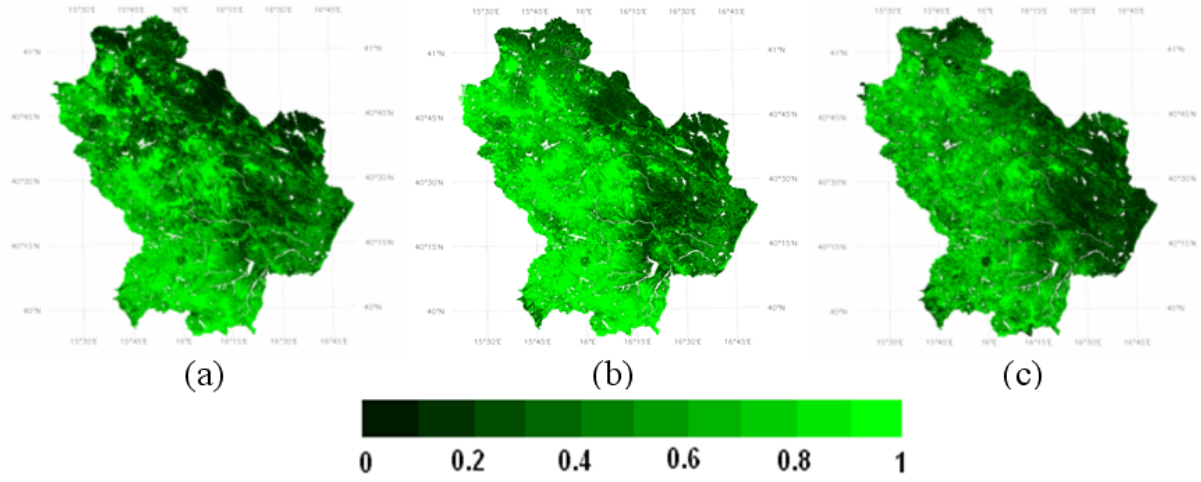


**Figure 3.** Vegetation cover, $P_v$, maps; (a) 09/26/1999, (b) 06/14/2002, (c) 05/26/2004.

### 2.1 Surface temperature and emissivity

Landsat-TM and ETM+ sensors possess a unique thermal band with a spectral range of 10.4 - 12.5 $\mu$m, and an effective wavelength of 11.457 $\mu$m. This limitation does not allow to apply split-window methods neither Temperature/Emissivity Separation (TES) methods. Therefore, a single-channel method, based on the radiative transfer equation, was used. The remotely measured channel radiance, $R_i$, consist of two main contributions: (1) the radiance at surface level, which is attenuated by the absorption of the atmosphere between the surface and the instrument, characterized by the atmospheric transmittance, $\tau_i$, and (2) the upwelling sky radiance emitted by the atmosphere in the viewing direction, $L^{\Uparrow}_{i\ atm}(\Theta)$, so that $R_i$, in agreement with the radiative transfer equation, is stated as:

$$R_i = [\varepsilon_i B_i(T_R) + [1-\varepsilon_i]L^{\Downarrow}_{i\ atm\ hem}]\tau_i + L^{\Uparrow}_{i\ atm} \qquad (4)$$

where $B_i(T_R)$ is Planck's function for a temperature $T_R$, $\varepsilon_i$ is the surface emissivity and $L^{\Downarrow}_{i\ atm\ hem}$ is the hemispheric downwelling sky irradiance divided by $\pi$ (Lambertian reflection assumed). Radiosounding data were introduced into the MODTRAN 4.0 code to get estimates of $\tau_i$, $L^{\Uparrow}_{i\ atm}(\Theta)$ and $L^{\Downarrow}_{i\ atm\ hem}$. Altough Equation 4 depends on the observation angle ($\Theta$), the nadir view provides good results for Landsat-TM and ETM+. A simple and operational equation proposed by Valor and Caselles (1996) was used to estimate the surface emissivity from the knowledge of the vegetation cover, $P_v$, and the emissivities of the soil and canopy components, $\varepsilon_s$ and $\varepsilon_c$, respectively. Typical emissivity values can be assumed for $\varepsilon_c$ (0.985) and $\varepsilon_s$ (0.960) (Rubio et al., 2003). Of course, errors in Equation 5 would be reduced if particular *in situ* measurements of $\varepsilon_c$ and $\varepsilon_s$ were available.

$$\varepsilon = \varepsilon_c P_v + \varepsilon_s(1-P_v)(1-1.74P_v) + 1.7372P_v(1-P_v) \qquad (5)$$

### 2.2 Vegetation cover

Bands 3 (0.63 - 0.69 $\mu$m) and 4 (0.76 - 0.90 $\mu$m) of TM and ETM+ were used to estimate the vegetation index NDVI (Normalized Difference Vegetation Index). Previously, visible and near- infrared bands were corrected of atmospheric effects using the radiosounding data and the MODTRAN 4.0 code. For this purpose, the at-surface channel reflectivity, $\rho_i$, is calculated with the following equation:

$$\rho_i = \frac{\pi(r_i - L^{\Uparrow}_{i\ atm})d^2}{\tau_i(ESUN_i \cos\alpha\tau(\alpha) + L^{\Downarrow}_{i\ atm\ hem})} \qquad (6)$$

where $\tau(\alpha)$ is the atmospheric transmissivity between the sun and the surface, $\alpha$ is the zenithal solar angle, $ESUN_i$ is the spectral solar irradiance on the top of the atmosphere, and $d$ is the Earth-Sun distance.

The spectral contrast between red and infrared bands, 3 and 4, respectively, allow us to discriminate between pixels with different vegetation composition via the mentioned NDVI:

$$NDVI = \frac{\rho_4 - \rho_3}{\rho_4 + \rho_3} \qquad (7)$$

Vegetation cover was obtained through the expression (Valor and Caselles, 1996):

$$P_v = \frac{1 - \dfrac{NDVI}{NDVI_s}}{1 - \dfrac{NDVI}{NDVI_s} - K\left(1 - \dfrac{NDVI}{NDVI_v}\right)} \qquad (8)$$

where the coefficient $K$ is obtained by:

$$K = \frac{R_{NIR_v} - R_{RED_v}}{R_{NIR_s} - R_{RED_s}} \qquad (9)$$

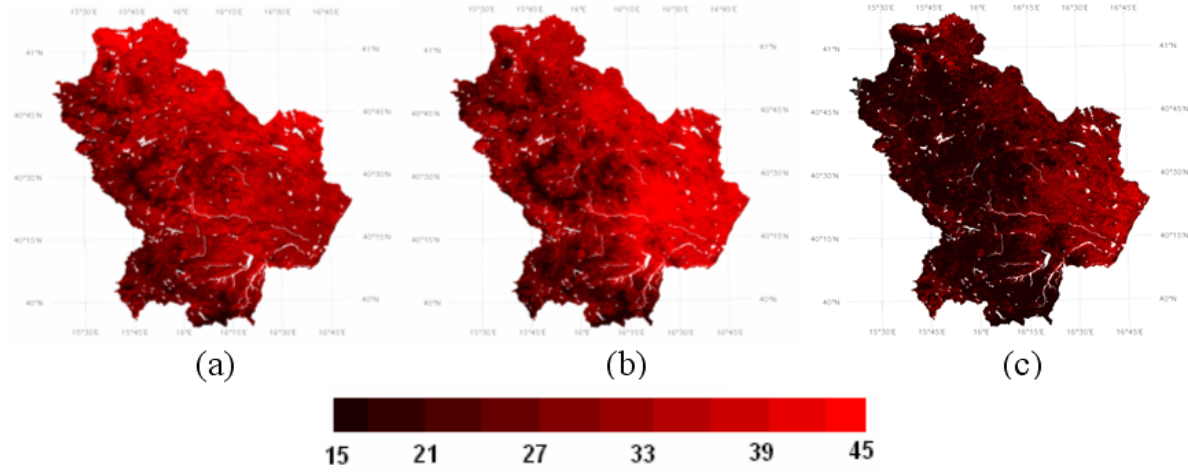


**Figure 4.** Land surface temperature, $T_R$ (°C), maps; (a) 09/26/1999, (b) 06/14/2002, (c) 05/26/2004.

where $R_{NIR}$ is the near infrared reflectivity, and $R_{RED}$ is the red visible reflectivity. The subscript $v$ and $s$ correspond to completely vegetated and unvegetated areas, respectively, selected by looking at the spectral contrast among bands 3 - 5. These selected areas were also used to estimate $T_c$ and $T_s$, required in the STSEB model (Sánchez et al., 2008), from the land surface temperature maps generated.

## 2.3 Albedo

Some authors such as Dubayah (1992) divided the spectral region from 0.3 to 3.0 $\mu$m into 10 spectral bands to estimate surface albedo. Each band has a different integrating weight according to the typical vegetation spectral reflectance pattern. In this paper, the surface albedo is integrated by using the equation (Dubayah, 1992):

$$\alpha = 0.221\rho_1 + 0.162\rho_2 + 0.102\rho_3 + 0.354\rho_4 + 0.059\rho_5 + 0.0195\rho_7 \quad (10)$$

where $\rho_i$ is the corrected reflectivity for the $i$ band of TM or ETM+. The average error of the calculated surface net radiation, using Equation 10 for estimating the albedo, is around 2% when comparing to field measurements (Dubayah, 1992).

## 2.4 Meteorological variables

Ancillary meteorological data are required to complete the set of variables and parameters involved in the previously shown scheme of equations. Air temperature, $T_a$, is necessary in the STSEB scheme (Sánchez et al., 2008) to estimate the exchange of sensible heat flux between the surface and the atmospheric boundary layer. Wind speed, $u$ (m s$^{-1}$), is required in the expressions to calculate the aerodynamic and soil resistances taking part in the STSEB model. The global solar radiation, $S$, and the incident long-wave radiation, $L_{sky}$, are necessary in the net radiation balance (Equation 3). Since all these variables, except $L_{sky}$, are continuously registered in typical agro-meteorological stations, regional maps can be created by interpolating the data registered in a network of stations distributed within the study area. Regarding $L_{sky}$, due to its known spatial homogeneity across a relative extensive area, a single value of this variable can be used for each image, and it can be obtained from launched radiosoundings. Note that additional information such as vapour pressure (necessary in the PM method) or soil moisture conditions (necessary in the PT method to estimate the PT constant) are not longer required. In this paper, a geostatistical technique (kriging) was used to interpolate the data of a regional network of agro-meteorological stations, and elaborate wind speed and global solar radiation maps. The kriging technique models spatial distribution as a function of observational data across a region without prior knowledge of the distribution of its underlying physical causes. Therefore, the main limitation of this interpolation method is the lack of robustness to local variations provoked by the terrain orography. Also, a critical point in the kriging process is to estimate the spatial covariance function or variogram (Cressies, 1991). A Digital Elevation Model (DEM) was considered and the relationship between the air temperature and the altitude above sea level was established in order to obtain more reliable maps of this meteorological variable. Analysis from meteorological models could be also used to create regional maps of the inputs required. However, the inaccuracies in the estimates using a model are bound to be higher than those from direct ground measurements, and may then lead to unacceptable errors in the flux estimates.

**Table 1.** Average values of $LE_d$ (W m$^{-2}$) for the main land uses.

| Land use | L7-ETM+ (09/26/1999) | L7-ETM+ (06/14/2002) | L5-TM (05/26/2004) |
|---|---|---|---|
| Pastures | 80 | 92 | 117 |
| Natural Grassland | 97 | 112 | 132 |
| Fruit trees | 106 | 140 | 123 |
| Olives | 94 | 117 | 117 |
| Vineyards | 92 | 129 | 120 |
| Moors and heathland | 92 | 106 | 117 |
| Sparsely vegetated areas | 74 | 66 | 103 |
| Arable lanas | 69 | 100 | 129 |
| Land princ. ocup. by agriculture | 103 | 126 | 134 |
| Annual crops | 92 | 117 | 126 |
| Complex cultivation patterns | 94 | 114 | 123 |
| Coniferous forests | 120 | 192 | 137 |
| Broad-leaf forests | 114 | 149 | 120 |
| Mixed forests | 77 | 109 | 109 |
| WHOLE REGION | 92 | 120 | 123 |

## 3 Application to the southern italian region of Basilicata

### 3.1 Description of the site, measurements, and satellite images.

Placed in the south of Italy, Basilicata is a 9992 km$^2$ region, divided in two provinces: Potenza and Matera (Figure 2a). It is a prevalently mountainous region. In fact, mountains take up the 47% of the territory (areas above 700 m above sea level), hills take up the 45% (areas between 201 and 700 m above sea level) and plains just the 8% (areas below 200 m a.s.l.). The western mountainous part of the region can be distinguished from the coastal and the hilly central ones, which extends as far as the arid *Murgia* of Matera. Figure 2b shows the DEM, obtained from MODIS, used in this work.

The wide variety of land uses in this region makes it appropriate for an analysis of the method performance in evapotranspiration retrieval under different surface conditions. A land use map from the CORINE Land Cover project (Figure 2c) was used to characterize the surface with nominal values of canopy height for each land use.

A network of 38 agro-meteorological stations distributed within the region and managed by ALSIA (Agenzia Lucana di Sviluppo ed Innovazione in Agricoltura - Agriculture Development and Innovation Agency of Lucania) are equipped with instruments for automatic and continuous measurements of various meteorological parameters, such as air temperature, relative humidity, global solar radiation, soil temperature, speed and direction of wind, precipitation and potential evapotranspiration. Air temperature is measured by PT100 thermo-resistances with a precision of 0.1°C. Solar radiation is measured through pyranometers working in the range 0.3 - 2.5 $\mu$m with an accuracy of 2%. The instruments used for the survey of the horizontal component of the wind speed are classic whirling arms, with an accuracy of 0.5 m s$^{-1}$.

Finally, two weighing lysimeters placed at two different cropland sites, Lavello (41°6'6"N, 15°50'55"E) and Policoro (40°10'15"N, 16°38'53"E), registered actual $LE_d$ values. These weighing lysimeters consist of a filled-in cultivation tank, with an area of 2 m x 2 m and a depth of 1.30 m, isolated from any external structure. Water consumptions and daily evapotranspiration are obtained directly by the difference in weight between two subsequent readings. The resolution of this system is about 0.06 mm. Experimental Demonstrative Farm of Gaudiano - Lavello provided us with *in situ* lysimeter data, collected by the University of Basilicata, corresponding to: September 26th 1999 and June 14th 2002, on an aubergine and tomato growing respectively. Evapotranspiration data corresponding to September 26th 1999, on a radish growing, and June 14th 2002, on a tomato growing, were provided by the Food Production Science Institute of Bari, which is responsible for collecting data coming from Experimental Farm "E. Pantanelli" of Policoro.

Three cloud-free Landsat images were selected for this work, one corresponding to the TM sensor, on-board Landsat 5, (hereafter referred to as L5-TM) (May 26th 2004), and two corresponding to the ETM+ sensor, on-board Landsat 7 (hereafter referred to as L7-ETM+) (September 26th 1999 and June 14th 2002). The high spatial resolution of these sensors (30-m in visible and near infrared bands, and 60-m for L7-ETM+ or 120-m for L5-TM in the thermal band) allows a detailed monitoring of the surface features, required in the methodology described, for the whole Basilicata region.

### 3.2 Results and discussion

Atmospheric profiles, from operational radiosoundings launched in a nearby area, were processed for each date using

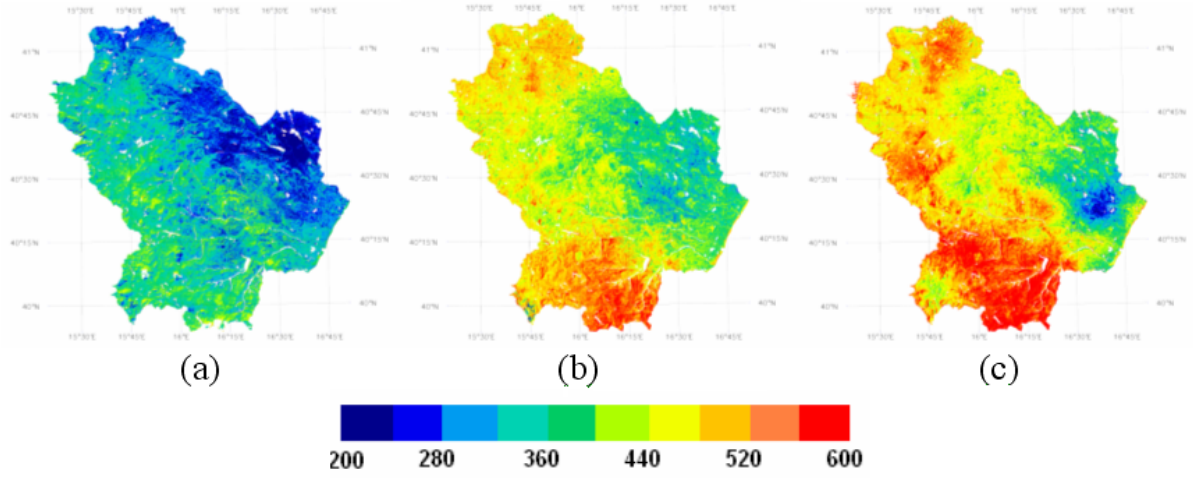


**Figure 5.** Instantaneous net radiation flux, $R_{ni}$ (W m$^{-2}$), maps; (a) 09/26/1999, (b) 06/14/2002, (c) 05/26/2004.

**Table 2.** Comparison between Lysimeter measurements of $LE_d$ (W m$^{-2}$) and results obtained for the particular locations of the instruments.

| Date | Lysimeter | Measured | Estimated | Diff. | Relative diff. |
|---|---|---|---|---|---|
| September 26th 1999 | Lavello | - | 86 | - | - |
| | Policoro | 54 | 60 | 6 | 11 |
| June 14th 2002 | Lavello | 63 | 92 | 29 | 50 |
| | Policoro | 83 | 86 | 3 | 3 |

the MODTRAN 4.0 code. As explained in Section 2.2, visible and near-infrared bands were corrected, and a NDVI map was elaborated from each Landsat image. A careful searching process was carried out, based on the contrast shown in bands 3 and 4, and on the obtained NDVI, so as to identify completely vegetated and completely bare pixels. Several samples of each class were selected and distributed around the whole region in order to account for the spatial variability within the area. Average values of these samples were used for the soil and canopy parameters in Equations 8 and 9. Figure 3 shows the vegetation cover maps obtained from the three images. Note that the image corresponding to June 2002 shows the highest $P_v$ values overall. Also, the highest $P_v$ values are easily identified with forested areas looking at Figure 2c. As explained in Section 2.1, emissivity maps were obtained by applying Equation 5 assuming nominal values of $\varepsilon_c$ = 0.985 and $\varepsilon_s$ = 0.960. Land surface temperature maps (Figure 4) were finally obtained by applying Equation 4. Some authors such as Sobrino et al. (2004) and Li et al. (2005) have shown the validity of the Land Surface Temperature (LST) obtained from Landsat 5-TM and Landsat 7-ETM+, respectively, using the radiative transfer equation, with errors lower than 1°C.

A linear regression was obtained between the available air temperature values and the altitude above sea level of the corresponding stations. The air temperature maps were obtained by applying this deduced relationship to the whole region from the DEM terrain altitude information. Root Mean Square Difference (RMSD) values close to 1°C were obtained when comparing the predicted $T_a$ values with the ground observations. A kriging interpolation was used to elaborate wind speed and global solar radiation maps as stated in Section 2.4.

Figure 5 shows the net radiation maps obtained through Equation 3. The integrated surface albedo was estimated using Equation 10. Previous emissivity results using Equation 5 were also used here. Comparing Figures 5 and 3, it can be seen that the highest $R_{ni}$ values are obtained for the most vegetated areas, and the lowest for the bare areas. After estimating the values of $T_c$ and $T_s$ according to the aforesaid procedure, sensible heat flux (Figure 6) was obtained through the STSEB approach (Sánchez et al., 2008). At the Landsat overpass times, $T_R$ is typically higher than $T_a$ for most landscapes (positive $H$). However, there are some cases in which $T_a > T_R$. Also, the produced maps of air temperature may contain spatial uncertainties yielding unrealistically high values of $T_a$. In these cases, negative $H_i$ values can be observed. Furthermore, a wider spatial heterogeneity is shown compared with the $R_{ni}$ maps. As a direct consequence, the spatial variability of the evapotranspiration will be mainly tied to the spatial distribution of the sensible heat flux. Finally, Figure 7 shows the $LE_d$ maps (mm day$^{-1}$) obtained by

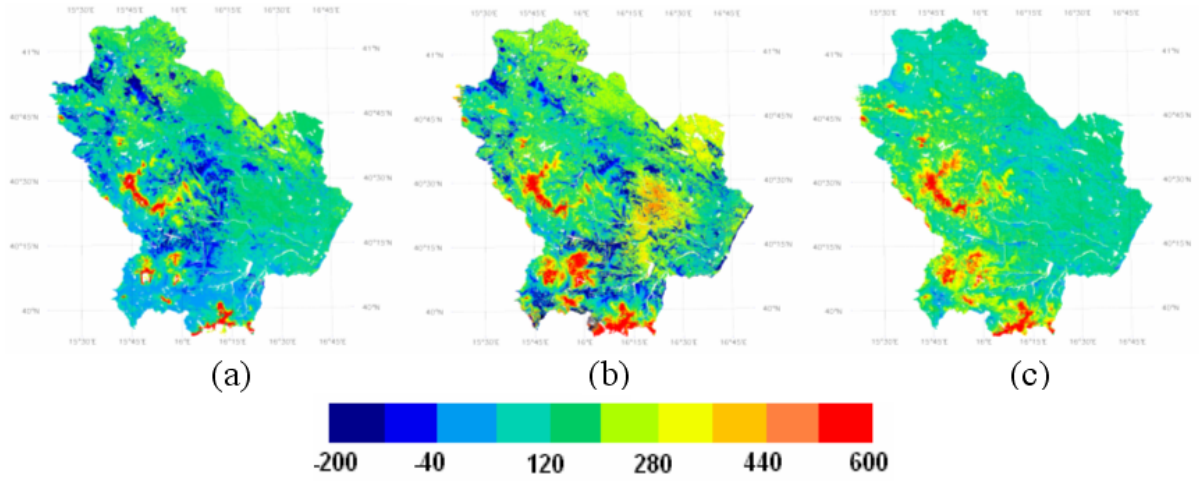


**Figure 6.** Instantaneous sensible heat flux, $H_i$ (W m$^{-2}$), maps; (a) 09/26/1999, (b) 06/14/2002, (c) 05/26/2004.

applying Equation 2 from the previous results. $R_{nd}/R_{ni}$ values were calculated for each date from the ground-collected data. Since the ratio $R_{nd}/R_{ni}$ has been shown to vary with the time, date, or the site latitude, but not with the vegetation type (Sobrino et al., 2005; Sánchez et al., 2007), a constant value was used for each image: 0.365, 0.378, and 0.351 for the images L7_99, L7_02, and L5_04, respectively. Overall, it can be seen that the highest $LE_d$ values were obtained for the most vegetated areas, while the lowest for the bare areas. However, there is also a small portion of pixels with high $P_v$ values and low $LE_d$ values. Those correspond to areas above approximately 1500 m altitude, according to the DEM. For a quantitative analysis of the regional $LE_d$ results, average values of all pixels within each land use have been calculated. Table 1 shows a list of these results for the main land uses.

Coniferous and broad-leaf forests, together with fruit trees and agriculture areas, show generally the highest values. Meanwhile, sparsely vegetated areas, arable lands, mixed forests or pastures show the lowest $LE_d$ values. Note the low variability in $LE_d$ results of the different land uses for the L5-TM image compared with the other two L7-ETM+ cases. The 120-m spatial resolution in the thermal band of TM, compared with the 60-m of ETM+, can be significant for this fact. Moreover, we can observe that the $LE_d$ results are clearly lower for the image of September than for the other two in May and June. Besides, the average $LE_d$ value for the whole Basilicata region resulted 92, 120, and 123 W m$^{-2}$ for the L7_99, L7_02, and L5_04 images, respectively. This seems to be logical taking into account the phenological stage of the vegetation for each date. However, no firm conclusion can be stated at this point since the three images correspond to different years, and conditions could have changed from one to the other.

To assess the performance of the described methodology, $LE_d$ results were compared with some punctual lysimeter measurements. Table 2 shows the comparison between these measurements and the results obtained in Figure 7 for the particular location of the two lysimeters. Unfortunately, the Lavello datum for September 26th 1999 was not reliable, and no lysimeter data were available for May 26th 2004. A RMSD value of 20 W m$^{-2}$ was obtained. To reinforce this assessment at a wider scale, data from the CarboEurope project dataset have been used. This is an international project whose main objective is the study of the carbon dioxide exchanges between the surface and the atmosphere. For this aim, a network of towers, equipped with the instruments required for the direct measurement of the surface fluxes, has been distributed around Europe. Table 3 shows the location of some towers placed in Italian territory, as well as information about the vegetation type over which they are located. Ground-measured $LE_d$ values from these towers, using eddy-correlation or Bowen ratio systems, were used to test the average values obtained using the land use classification over the Basilicata region. A RMSD value of 30 W m$^{-2}$ is obtained with an overestimation of 17 W m$^{-2}$. Note that the most significant differences are obtained for the coniferous forest sites. Even though a more complete network of $LE_d$ ground-measured values, spatially distributed around the study region and representative of the different land uses, would be desirable for a robust validation, the results obtained give some confidence on the proposed methodology to evaluate daily evapotranspiration at a regional scale.

Note that the main aim of the present work is to show a feasible and, at the same time, simple and operational methodology that allows us to retrieve $LE_d$ at a regional scale assembling remote sensing and ground-measured data. More complicated techniques, involving a greater number of variables and parameters, and/or more tedious computation processes could have been introduced. However, the operationality of the method would have been significantly re-

**Table 3.** Comparison between ground-measured values of $LE_d$ (W m$^{-2}$) in the CarboEurope Italian sites and results obtained for similar land uses over the Basilicata region.

| Site/Date | Land cover | Lat./Long. | $LE_d$ measured | $LE_d$ estimated | Diff. | Relative diff. (%) |
|---|---|---|---|---|---|---|
| Collelongo | Mixed forest | 41°0'58"N | 57 | 77 | 20 | 30 |
| 09/26/1999 | | 13°5'17"E | | | | |
| San Rossore | Coniferous forest | 43°43'47"N | 134 | 192 | 57 | 40 |
| 06/14/2002 | | 10°7'13"E | | | | |
| Roccaresp. 1 | Broad-leaf forest | 42°4'29"N | 126 | 149 | 23 | 18 |
| 06/14/2002 | | 11°5'48"E | | | | |
| Roccaresp. 2 | Broad-leaf forest | 42°23'25"N | 120 | 149 | 29 | 24 |
| 06/14/2002 | | 11°55'15"E | | | | |
| Castelpolziano | Natural grassland | 42°35'8"N | 80 | 112 | 31 | 40 |
| 06/14/2002 | | 10°4'44"E | | | | |
| Nonantola | Cropland | 44°41'23"N | 154 | 126 | -29 | 19 |
| 06/14/2002 | | 11°5'19"E | | | | |
| Lavarone | Coniferous forest | 45°57'19"N | 97 | 137 | 40 | 40 |
| 05/26/2004 | | 11°16'52"E | | | | |
| Parco Ticino | Broad-level forest | 45°12'3"N | 143 | 120 | -23 | 16 |
| 05/26/2004 | | 9°3'40"E | | | | |
| Monte Bond. | Mixed forest | 46°1'47"N | 112 | 109 | -3 | 3 |
| 05/26/2004 | | 11°4'59"E | | | | |
| | | | | Bias | +17 | |
| | | | | $\sigma$ | 30 | |
| | | | | RMSD | 30 | |

duced. Further work will deal with the study of the effect of possible improvements to the described methodology on the final $LE_d$ results. For example:

- More sophisticated methods that incorporate geographical information, such as co-kriging and elevation- detrended kriging techniques can be applied to elaborate maps of the meteorological variables required. Also, a digital elevation model with a higher spatial resolution can be introduced to reduce errors in the interpolation of the air temperature.
- Recent works have dealt with the effects of subpixel heterogeneity on the fluxes estimation, and a disaggregation procedure has been proposed for estimating subpixel variations in radiometric surface temperature (Kustas et al., 2003). This technique can be applied to Landsat images and derive $T_{rad}$ at the NDVI pixel resolution (30 m). Particular interest has the application of this procedure to L5-TM images because of the low contrast shown in the $LE_d$ results.
- Specific values of soil and canopy emissivities could be assigned to the different land use classes. In this way, emissivity values more representative of the real local vegetation and conditions could be used in the emissivity correction of the radiometric temperature. Also, unique values of $T_c$ and $T_s$ have been used for the whole region in the sensible heat fluxes retrieval. An estimation of these values for the different land uses could account for possible differences.

## 4 Conclusions

In this work, an operational methodology to estimate actual daily evapotranspiration at a regional scale, assembling remote sensing techniques and micro-meteorology, is presented. The traditional relation of Itier and Riou (1982) is combined with the proposed STSEB micro- meteorological model (Sánchez et al., 2008), with the aim of retrieving $LE_d$ values from single information at a particular day time. The STSEB model has been introduced to estimate surface energy fluxes over sparse and heterogeneous canopies from radiometric surface temperatures and micro-meteorological data.

As a particular example, in this work the method is applied to the Basilicata region, in the South of Italy, using Landsat imagery. Three images acquired in different dates are used, two from Landsat 7-ETM+, and one from Landsat 5-TM. The CORINE Land Cover map and a complete network of agro-meteorological stations provide the set of ground variables and parameters required to apply the methodology. Maps of the different surface fluxes are built up. An analysis of the $LE_d$ results is made taking the land use classification as a basis, and differences between the different types of vegetation and dates are stated. Overall, the highest $LE_d$ values correspond to the most vegetated areas. It is important to point out that the spatial variability of the evapotranspiration is mainly tied to the spatial distribution of the sensible heat flux due to its wider heterogeneity shown in comparison with the net radiation results. The performance of the method at both local and regional scale is assessed by comparing the results with some ground measurements. An estimation error close to 30 W m$^{-2}$ is finally obtained.

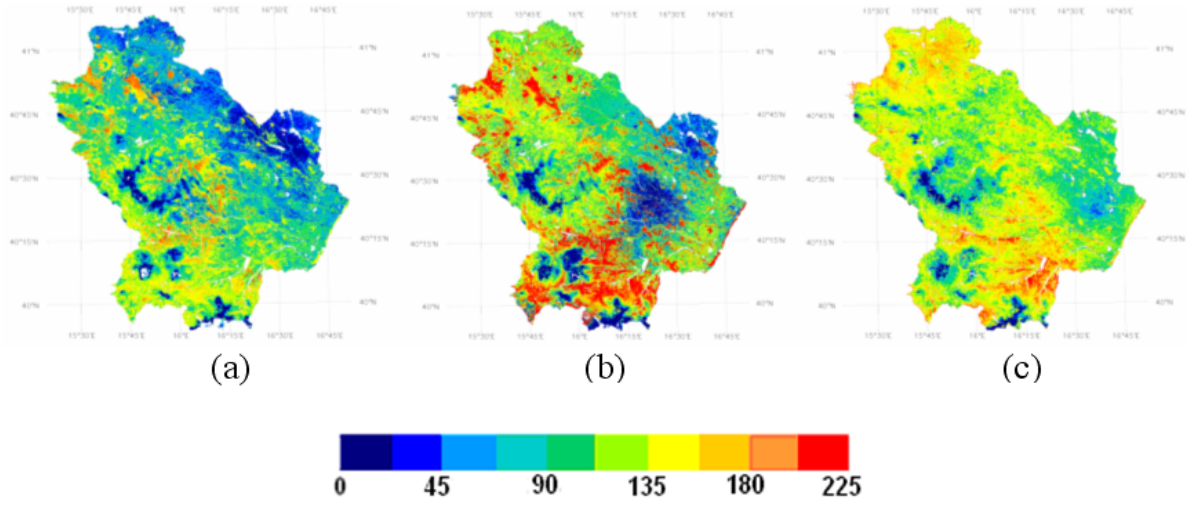


**Figure 7.** Actual daily evapotranspiration, $LE_d$ (W m$^{-2}$), maps; (a) 09/26/1999, (b) 06/14/2002, (c) 05/26/2004.

The methodology presented in this work can be expanded and applied to any other region worldwide and to other satellite sensors. The only requirements are appropriate registers of instantaneous air temperature, wind speed and solar radiation concurrent with the satellite overpass, and, of course, at least one satellite image of the day we are interested in. The possibility of using numerical models to substitute the ground measurements, and thus account for the lack of meteorological stations, needs further investigation. The effect of the modelled input uncertainties on the flux results must be analyzed. Despite this fact, we believe that the work has the potential to present a valuable contribution to the monitoring of surface evapotranspiration and water requirements, as well as to water management tasks.

**Acknowledgements.** This work was funded by the *Ministerio de Educación y Ciencia* (Projects CGL2004-06099-C03-01 and CGL2007- 64666/CLI, co-financed with European Union FEDER funds, *Acciones Complementarias* CGL2005-24207-E/CLI and CGL2006- 27067-E/CLI), and the University of Valencia (*V Segles* Research Grant of Mr. J. M. Sánchez). Also, the authors express their gratitude to *ALSIA* (*Agenzia Lucana per lo Sviluppo ed Innovazione in Agricoltura*) for providing field data, and to IMAA (*Istituto di Metodologie per l'Analisi Ambientale*) of CNR (*Consiglio Nazionale delle Ricerche*), and Tito Scalo for providing the base elaborations of satellite images. Valuable comments and suggestions of Drs. Enric Valor and César Coll (University of Valencia) to previous versions of this work are highly appreciated.

## References

Allen, R. G., Pereira, L. S., Raes, D., and Smith, M., 1998: Crop evapotranspiration: guidelines for computing crop water requirements, FAO Irrigation and Drainage Paper, 56, Rome, 300 pp.

Büttner, G., Feranec, J., and Jaffrain, G., 2002: Corine Land Cover update 2000: Technical guidelines, European Environment Agency, Copenhagen.

Cressies, N., 1991: Statistics for spatial data, John Wiley and Sons, New York.

Dubayah, R., 1992: *Estimating net solar radiation using Landsat Thematic Mapper and digital elevation data*, Water Resour Res, **28**, 2469–2484.

Itier, B. and Riou, C., 1982: *Une nouvelles méthode de determination de l'évapotranspiration réelle par thermographie infrarouge*, J Rech Atmos, **2**, 113–125.

Kustas, W. P., Norman, J. M., Anderson, M., and French, A., 2003: *Estimating subpixel temperatures and energy fluxes from the vegetation index-radiometric temperature relationship*, Remote Sens Environ, **82**, 429–440.

Li, F., Kustas, W. P., Prueger, J. H., Neale, C. M. U., and Jackson, J. J., 2005: *Utility of Remote Sensing Based Two- Source Energy Balance Model Under Low and High Vegetation Cover Conditions*, J Hydrometeorol, **6**, 878–891.

Rubio, E., Caselles, V., Coll, C., Valor, E., and Sospedra, F., 2003: *Thermal-infrared emissivities of natural surfaces: improvements on the experimental set-up and new measurements*, Int J Remote Sens, **24**, 5379–5390.

Sánchez, J. M., Caselles, V., Niclòs, R., Valor, E., Coll, C., and Laurila, T., 2007: *Evaluation of the B-method for determining actual evapotranspiration in a boreal forest from MODIS data*, Int J Remote Sens, **28**, 1231–1250.

Sánchez, J. M., Caselles, V., and Kustas, W. P., 2008: *Estimating surface energy fluxes using a micro-meteorological model and satellite images*, Tethys, **5**, DOI: 10.3369/tethys.2008.5.03.

Sobrino, J. A., Jiménez-Muñoz, J. C., and Paolini, L., 2004: *Land surface temperature retrieval from LANDSAT TM 5*, Remote Sens Environ, **90**, 434–440.

Sobrino, J. A., Gómez, M., Jiménez-Muñoz, J. C., Olioso, A., and Chehbouni, G., 2005: *A simple algorithm to estimate evapotranspiration from DAIS data: Application to the DAISEX campaigns*, J Hydrol, **315**, 117–125.

Valor, E. and Caselles, V., 1996: *Mapping land surface emissivity from NDVI. Application to European, African and South-American areas*, Remote Sens Environ, **57**, 167–184.